Ceramics International 50 (2024) 19217–19227

Contents lists available at ScienceDirect

Ceramics International

journal homepage: www.elsevier.com/locate/ceramint

Influence of graphene-based nanostructures processing routes and aspect ratio in flexural strength and fracture mechanisms of 3Y-TZP-matrix composites

R. Moriche [a,*], E. Guisado-Arenas [a], C. Muñoz-Ferreiro [a,b,c], C. López-Pernía [a], A. Morales-Rodríguez [a], E. Jiménez-Piqué [d], Á. Gallardo-López [a], R. Poyato [b]

[a] Departamento de Física de la Materia Condensada, ICMS, CSIC-Universidad de Sevilla, Apdo. 1065, 41080, Sevilla, Spain
[b] Instituto de Ciencia de Materiales de Sevilla, ICMS, CSIC-Universidad de Sevilla, Avda. Américo Vespucio 49, 41092, Sevilla, Spain
[c] CNRS, INSA Lyon, Universite Claude Bernard Lyon 1, MATEIS, UMR5510, 69621, Villeurbanne, France
[d] Center for Structural Integrity, Reliability, and Micromechanics of Materials (CIEFMA), Department of Materials Science and Engineering, Universitat Politècnica de Catalunya (UPC) - BarcelonaTECH, 08019, Barcelona, Spain

ARTICLE INFO

Handling editor: Dr P. Vincenzini

Keywords:
B. Nanocomposites
C. Mechanical properties
C. Strength
C. Fracture

ABSTRACT

In this work, the influence of the aspect ratio of graphene-based nanostructures (GBNs) and content on the mechanical properties of 3 mol% yttria tetragonal zirconia polycrystalline 3Y-TZP matrix composites was analysed. The influence of the dispersion method and sintering parameters on the flexural strength and elastic modulus of the composites was studied, and the fracture surfaces were characterized to determine the fracture mechanisms that occur. The results showed that small amounts of exfoliated graphene nanoplatelets, with reduced lateral size, and few layer graphene, up to 1.0 and 2.5 vol%, respectively, slightly increase the 3Y-TZP flexural strength. This has been attributed to the tortuosity of the crack propagation pathways and strengthening mechanisms. Higher contents cause a decrease in flexural strength and stiffness because of overlapped GBNs, which can promote the crack propagation. The pull-out of GBN was more significant in composites with non-exfoliated graphene nanoplatelets, where no increase on the flexural or biaxial strength was measured.

1. Introduction

Yttria-stabilized tetragonal zirconia polycrystals (Y-TZP) are well known for their significant role as advanced structural ceramics in technological applications. Due to its high strength, fracture toughness, and stability at high temperature, among others, it is one of the key materials used as structural components in engines [1], machining and cutting tools [2], and one of the most utilized materials as biomedical implants [3]. During the last decades, research has focused on the incorporation of nanostructured reinforcements, which can induce an enhancement of the electrical, thermal, mechanical, and tribological properties [4] of ceramic materials, including Y-TZP. This fact leads to enabling other functionalities, which makes possible to expand the field of applications, and the processing and machining routes, traditionally limited for ceramic materials [5,6]. Nonetheless, if the addition of these nanostructured fillers induces detrimental effects in the mechanical properties of Y-TZP, their application would be restricted to non-structural applications. Being the Y-TZP an advanced structural ceramic, it is essential to deeply understand how the nanofiller affects mechanical performance.

In particular, the addition of carbon-based fillers, due to their electrical and thermal properties, to ceramic matrices has received special attention [7–10]. As an example, Kishimoto et al. [11] proposed the addition of carbon-black to an alumina matrix to develop pressure sensors based on changes in electrical resistivity of the bulk material. Waku et al. [12] also proposed the incorporation of graphite as a second phase in alumina-matrix composites to make the material piezoresistive. Among carbon-based nanofillers, graphene-based nanostructures are especially promising [13]. Zhou et al. [14] suggested the use of a porous graphene/Al_2O_3 ceramic for heat transfer and thermal energy storage and directional architectures to improve thermal conductivity [15]. Muñoz-Ferreiro et al. [16] have demonstrated that the incorporation of different graphene-based nanostructures (GBNs) into a polycrystalline matrix of 3 mol% yttria tetragonal zirconia (3Y-TZP) achieves high

* Corresponding author.
E-mail address: rmoriche@us.es (R. Moriche).

https://doi.org/10.1016/j.ceramint.2024.03.021
Received 5 December 2023; Received in revised form 23 February 2024; Accepted 3 March 2024
Available online 4 March 2024

efficiency in the electrical discharge machining (EDM) due to their high electrical conductivity.

Additionally, GBNs have been reported to enhance the mechanical behaviour of several ceramics due to toughening mechanisms such as pull-out, crack bridging, and deflection [17]. Markandan et al. [18] have reported that contents below 2 wt% (~5 vol%) graphene-based second phases homogeneously dispersed give rise to crack deflection, crack bridging, and crack branching, inducing hardening and toughening in zirconia. Chen et al. [19] obtained fracture toughness and hardness enhancement for graphene nanoplatelet (GNP) contents less than 0.05 wt% (~0.1 vol%) in zirconia matrix composites. Liu et al. [20] also described the hardening and toughening of 3Y-TZP ceramic matrices by the addition of GNPs up to 1.0 vol%.

Related to the flexural strength of these GBN-based composites, different tendencies have been reported. Cui et al. [21] observed a slight increase (<10%) in the flexural strength of Al_2O_3/TiB_2 with 0.3 wt% (~0.8 vol%) of GNP prepared by spark plasma sintering (SPS). Li et al. [22] studied the influence of the incorporation of GNP contents ranging from 0.25 up to 1.0 vol% in Al_2O_3 ceramics densified by SPS and high-frequency induction heated dual sintering (SPS–HF). They observed that an addition of GNP below 0.5 vol% induced an increase of 15.3% in flexural strength. Above this value, the flexural strength decreased. Sun et al. [23], despite of obtaining 25% enhancements in fracture toughness, have published diminutions in flexural strength when incorporating 0.1 wt% (~0.3 vol%) of reduced graphene oxide (rGO) into Al_2O_3 matrices. Gao et al. [10] also used rGO (0.25–1.0 wt%, ~0.7–2.6 vol%) to modify the mechanical behaviour of ZnO. They observed an increase in flexural strength from 38 ± 4 to 78 ± 3 MPa (~105%) when adding 0.5 wt% (~1.3 vol%) and a decrease down to 51 ± 3 MPa (~35%) by adding 1.0 wt% (~2.6 vol%). Pereira et al. [24] studied multilayered graphene (MLG)/Al_2O_3 composites with contents between 0.5 and 1.25 wt% (~1.3 and 3.3 vol%). For all compositions, a decrease in flexural strength was reported, being ~37% for 1.25 wt% (~3.3 vol%). Wu et al. [25] reported the effect of the nanofiller content (0.5 up to 2.0 wt%) on rGO/3Y-TZP prepared by SPS. Composites showed an enhancement of the flexural strength below 1.0 wt% (~2.6 vol%) and above it, there was a considerably decrease. Zhang et al. [26] also observed an inflection point in both flexural strength and fracture toughness at 0.15 and 0.10 wt% (~0.4 and 0.3 vol%), respectively, in rGO/3Y-TZP composites.

These and other published works [26,27] have shown different tendencies in flexural strength that occur with the addition of graphene-based nanofillers. Generally, the differences observed in mechanical properties are related to differences in the aspect ratio of the fillers, dispersion methods, and processing parameters. Different dispersion methods can cause exfoliation, folding, and breakage of GBNs [28], what would lead to differences in the microstructure of the sintered composite material and, consequently, differences in the mechanical behaviour. Although some works reporting the strength of these composites have been published, the number of published data is very scarce.

The aim of this work is to analyse the influence of the incorporation of four different GBNs -in contents ranging from 1 up to 5 vol%- in the flexure strength of 3Y-TZP. The dependence of flexural strength, elastic modulus, fracture mechanisms, and biaxial strength on processing parameters (i.e., dispersion process), and sintering conditions (sintering temperature and heating rate) is also studied, as they strongly influence the microstructure and, consequently, the mechanical response.

2. Materials and methods

2.1. Materials

The ceramic powder used was polycrystalline 3 mol% yttria tetragonal zirconia (ref. TZ-3YB-E, *Tosoh Corporation*, Tokyo, Japan) with an average particle size of 40 nm. Graphene nanoplatelets (GNPs) with an average lateral size below 5 μm and thickness in the range of 10–20 nm were purchased from *Angstron Materials* (ref. N006–P, Dayton, Ohio, USA). Few layers graphene (FLG) with an average lateral size below 10 μm and thickness in the range of 1 nm were also acquired from *Angstron Materials* (ref. N002-PDR-HD, Dayton, Ohio, USA).

2.2. Dispersion and sintering processes

Based on previous studies [28,29], four different dispersion processes were used to prepare GBN-based nanocomposites. Additionally, different GBN contents (1.0, 2.5 and 5.0 vol%) were added to study the influence in mechanical properties.

The dispersion of GNPs and 3Y-TZP was carried out by dry ball milling, in a high energy planetary ball mill (*Pulverisette 7*, *Fritsch classic line*, *Fritsch*, Germany), without any solvent, using a powder-to-ball weight ratio of 1:30 and a speed of 350 rpm for 4 h. Continuous probe sonication (*Model KT-600*, *Kontes Inc.* Vineland, NJ) was used as a second route to prepare GNP/3Y-TZP mixtures. In this case, isopropanol was used as a solvent, and dispersion was carried out with an amplitude of 95% and a frequency of 20 Hz for 20 min. Cycles of 5 min were applied to refrigerate and avoid heating of the mixture. Subsequently, the solvent was evaporated at 100 °C under magnetic stirring to obtain the dry powder.

A mixture of the powder used to obtain FLG-based nanocomposites was prepared by two different methods: wet ball milling in a high energy planetary ball mill (*Pulverisette 7*, *Fritsch classic line*, *Fritsch*, Germany) and bath sonication (*Clifton*™, *Fischer Scientific S.L.*, Madrid, Spain). In the first method, a mixture of tert-butanol/water (10 vol%) was used as solvent, the powder-to-ball weight ratio was 1:20 and the speed was 150 rpm during the first 15 min and held at 350 rpm for 4 h. In bath sonication, ethanol was used as solvent and a power of 160 W was applied for 30 min. Subsequently, the solvent was evaporated at 100 °C under magnetic stirring to obtain the dry powder.

The sintering was carried out at 1250 °C for 5 min under uniaxial pressure of 75 MPa by spark plasma sintering (SPS, Model 515S, *Dr Sinter Inc. Kanagawa*, Japan at the *University of Seville Research, Technology and Innovation Centre*, CITIUS). The heating and cooling rates were 300 and 50 °C/min, respectively. A sintering temperature of 1300 °C and a heating rate of 100 °C/min were applied to specific composites to assess their influence on mechanical performance. Table 1 shows the notation for all samples included in the study.

2.3. Microstructural characterization

Microstructural features and fracture surfaces were analysed by field-emission gun scanning electron microscopy (FEGSEM), particularly, a *FEI TENEO* from CITIUS.

The characteristic length of the GBNs (L_{GBN}) was measured by using

Table 1
Nomenclature and parameters used for the processing and sintering of GBN-based composites.

Filler	Sample	GBN content (vol%)	Dispersion method	Sintering parameters	
				Temperature (°C)	Heating rate (°C/min)
FLG	FLG	0.1, 1, 2.5, 5	Bath sonication	1250	300
	FLG-1300	2.5		1300	300
	m-FLG	2.5	Wet milling	1250	300
	m-FLG-100	2.5		1250	100
GNP	e-GNP	1, 2.5, 5	Dry milling	1250	300
	GNP	1, 2.5, 5	Probe sonication	1250	300

ImageJ as the length, i.e. caliper diameter, of individual or stacked GBNs observed in polished cross-sections. This is a key parameter to analyse possible interlocking of grains during fracture in a particular plane. The grain boundary length (L_{GB}) of the 3Y-TZP matrix corresponds to the perimeter calculated from the planar grain size considering equiaxial grains.

2.4. Mechanical properties

Flexural tests, in 3-point bending configuration, were performed by an adapted method based on ASTM C1161-13 on samples with dimensions 15 x 2.5 × 2 mm^2 using a spam of 10 mm and a crosshead speed of 0.5 mm/min in an *Instron 1165* machine. The surface subjected to tensile stress was polished to 1 μm, and the edges were chamfered with a 3 μm paste. At least, five tests were performed per material and all the tests were performed applying the load parallel to the compaction axis. After testing, the fracture surfaces were evaluated by confocal microscopy (*Leica, DCM3D*) and FEGSEM (*FEI TENEO,* CITIUS). The roughness parameters, specifically the arithmetical average height (R_a) and the ten-point height (R_z) were estimated from 3D profilometry.

Additionally, the elastic modulus was measured using the impulse excitation technique following the ASTM E1876 standard in samples with a diameter of 15 mm, utilizing a *Sonelastic*® equipment and software (*ATCP Physical Engineering*, Ribeirão Preto, Brazil).

Ball on three ball (B3B) tests, specific for brittle materials, were carried out in selected samples. The flexural radius was 6.35 mm, with a ratio of the support radius (R_a) to the disc radius (R), $R_a/R = 0.80$ using a universal test machine (*Instron 1341*).

3. Results and discussion

3.1. Microstructural features of the sintered composites

Among the parameters that can condition the mechanical properties of ceramics and ceramic matrix composites, the relative density, the grain size distribution, and the average planar grain size can be highlighted. There were no significant differences in the relative density and grain size distribution for the different samples in this study. In all samples, the achieved relative density was above 99%. Likewise, all planar grain sizes were found to be in the range of 0.25–0.30 μm; the composite materials showed slightly, but not substantially, lower values than that of the monolithic 3Y-TZP. The most remarkable diminution was shown by the e-GNP materials.

Other key factors, independently of the nature of the matrix, are how the filler is dispersed and distributed throughout the matrix, -i.e. the filler dispersion degree and orientation-, and the filler geometry and aspect ratio.

The strong dependence on the lateral size and the existence of a size effect on the mechanical behaviour of graphene-based nanocomposites has been previously reported not only for ceramics but also for polymer and metal matrix composites [30]. Additionally, it has been published that there is a critical lateral size for effective reinforcement of these nanofillers [31].

To elucidate the mentioned microstructural features, Fig. 1 shows SEM micrographs of representative cross-sectional areas corresponding to the studied GBN-based nanocomposites with a filler content of 5 vol %. It can be seen that the GBNs are homogeneously dispersed and randomly orientated in the case of the GNP-based composites prepared by dry milling, i.e., e-GNP (Fig. 1a). Furthermore, compared to the other nanostructures used in this paper, these GBNs have shorter characteristic length (<3 μm, Table 2). This fact has been deeply analysed in a previous published work [29] and is attributed to the high energy of the dispersion process, which causes breakage and fragmentation of nanoplatelets to characteristic lengths less than 3 μm, and significant exfoliation. Consequently, the mean free path, defined as the linear free space between adjacent nanoplatelets, in this particular case (e-GNPs), is considerably smaller relative to the other composites, as can be seen in Fig. 1.

In contrast, when the same GNPs are dispersed using probe sonication (Fig. 1b), the original lateral size is not significantly modified, and a bimodal distribution with two maxima in 2 and 10 μm is obtained. This implies longer mean free paths between adjacent GNPs, for the

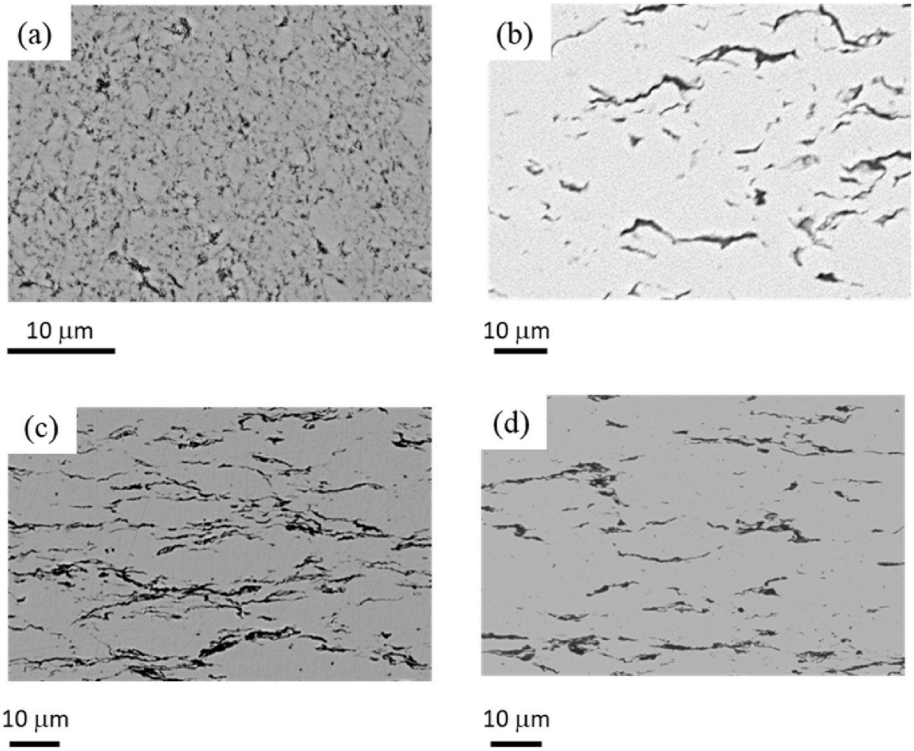

Fig. 1. Cross-sectional microstructure of (a) e-GNP, (b) GNP, (c) FLG, and (d) *m*-FLG-3-YTZP composites (5 vol%).

Table 2
Characteristic microstructural parameters and flexural strength of GBN-based nanocomposites.

Composite	GBN content (vol%)	GBN characteristic length, L_{GBN} (μm)			Flexural Strength (MPa)	Maximum flexural strength (MPa)	Weibull distribution	
		Min.	Max.	Mean (std.dev.)			Scale parameter (α)	Shape parameter (β)
3YTZP	–	–	–	–	950 ±180	1147	1005	8
FLG	0.1	0.22	30.40	1.81 (3.22)	1000 ±170	1132	1064	8
	1				970 ±170	1163	1020	10
	2.5				980 ±270	1304	1044	6
	5				720 ±150	903	767	8
FLG-1300	2.5				790 ±50	845	805	21
m-FLG	2.5	0.64	27.37	3.77 (4.45)	810 ±260	1089	878	5
m-FLG-100	2.5				820 ±130	919	861	12
e-GNP	1	0.22	2.60	0.54 (0.34)	1030 ±100	1137	1063	15
	2.5				770 ±100	901	806	9
	5				580 ±100	662	612	9
GNP	1	0.49	29.55	3.77 (4.11)	770 ±160	948	816	8
	2.5				800 ±120	933	837	10
	5				750 ±110	869	789	11

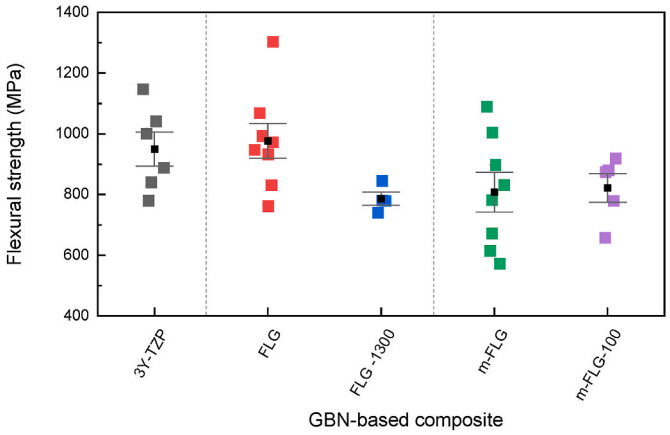

Fig. 2. Flexural strength of the composites with FLG (2.5 vol%) processed and sintered under different conditions. reference 3Y-TZP is included for comparison.

same nanofiller content, and larger isolated ceramic areas without nanofiller. Another relevant issue is that there is a preferential orientation of the GNPs perpendicular to the compaction axis, leading to an anisotropic material [29]. Additionally, the waviness of the GNPs can be clearly noted, which can be attributed to their high aspect ratio.

For FLG-based nanocomposites, samples prepared by bath sonication (Fig. 1c) showed dispersed FLGs with no significant reduction in lateral size compared to raw FLG, and with preferential orientation, perpendicular to the compaction axis. An in-depth study of the distribution, crystallinity of FLG, and the presence of defects in these composites has previously been published [32]. In that work, a reduction of defects in the FLG structure after sintering was reported. Due to their lower thickness and larger lateral size, the effective number of individual FLGs is greater than that related to GNPs for a given nominal content, leading to a more connected network and, thus, to a lower mean free path between the nanostructures and, also, to smaller filler-free 3Y-TZP areas.

In composites filled with FLG dispersed via wet milling (*m*-FLG), the separation of agglomerated FLGs seems to be not as effective as in the case of employing bath sonication and, consequently, it results in lower interconnectivity between the FLGs, i.e. higher mean free paths and larger GBN free ceramic areas. The resultant microstructure is more similar to that of the composites incorporating GNPs, with the difference that the FLGs are thinner and have a higher aspect ratio.

One of the morphological features that can be useful to explain how the lateral size of GBNs affects the mechanical properties of the ceramic composites is the characteristic length (L_{GBN}) of the GBN, mentioned above, and its magnitude compared to the grain boundary length (L_{GB}), defined in section 2.3 [33]. If the L_{GBN} is higher than the L_{GB}, each nanostructure will surround a group of grains, promoting specific strengthening mechanisms due to interlocking. In contrast, if the L_{GBN} is lower than the L_{GB}, the GBN is smaller than the perimeter of the grains and the mentioned interlocking will not occur. The L_{GB} of the studied materials were in the range of 0.6–1.0 μm. Table 2 shows the L_{GBN} for the composites analysed in this section. The minimum, maximum, and mean values of the L_{GBN} are included. Although the mean L_{GBN} values for FLG, *m*-FLG, and GNP-based composites are lower than the L_{GB}, the maximum value is considerably higher (~30 μm). This fact can also be elucidated in Fig. 1. On the contrary, the L_{GBN} for e-GNP-filled materials is considerably lower than the L_{GB}, with maximum and mean L_{GBN} values of 2.6 and 0.54 μm, respectively.

3.2. Mechanical properties

3.2.1. Influence of the processing route and SPS parameters

As mechanical properties have shown to be strongly dependent on microstructure due to the different processing route and sintering parameters, an analysis of how the dispersion method and sintering temperature affect the flexural strength of the FLG-based composites has been carried out in samples filled with 2.5 vol% with different processing and sintering conditions (available in Table 1). The results obtained from the flexural tests performed are shown in Fig. 2, where reference 3Y-TZP has also been included for comparison.

Regarding the sintering parameters, it can be seen that the flexural strength (980 ± 270 MPa) and the Weibull shape parameter (β) of the 2.5 vol% FLG samples, which have been sintered at 1250 °C and are electrically insulators [34], are similar to those of the 3Y-TZP ceramic. One issue worth noting is that, although the average value is similar, the values of the maximum flexural strength values obtained for each batch were 1304 and 1147 MPa, respectively (Table 1). This fact shows that the addition of FLGs into the ceramic matrix can effectively contribute to the strengthening of the material, also supported by the increase in the scale parameter (α) of the Weibull distribution.

In contrast to this result, the use of a higher sintering temperature (1300 °C), which makes the material electrically conductive [34] and, consequently, enables multifunctionality, decreases the flexural strength of the composite related to monolithic ceramic (~17%), obtaining a maximum value of 845 MPa in the best case. This could be caused by a slight increase in the grain size (from 0.39 ± 0.19 and 0.48 ± 0.15 μm, respectively) and residual stresses. This is supported by Raman spectra, which has been extensively discussed in a previous work [32]. A shift to higher frequencies, more significant in the 2D band, in the Raman spectra of the composites compared to raw FLG was reported, which is indicative of compressive residual stresses. It is well known that a residual compressive stress can contribute to enhance the mechanical resistance. As the composites sintered at 1250 °C showed higher values of Raman shifts, FLG should be subjected to higher compressive stresses compared to the composites sintered at 1300 °C, which could be the reason for the differences obtained in flexural strength. The flexural strength also decreases when wet milling is used as processing route (*m*-FLG and *m*-FLG-100) compared to the 3Y-TZP (Fig. 2 and Table 1). The decrease observed in this case is probably due to the poorer

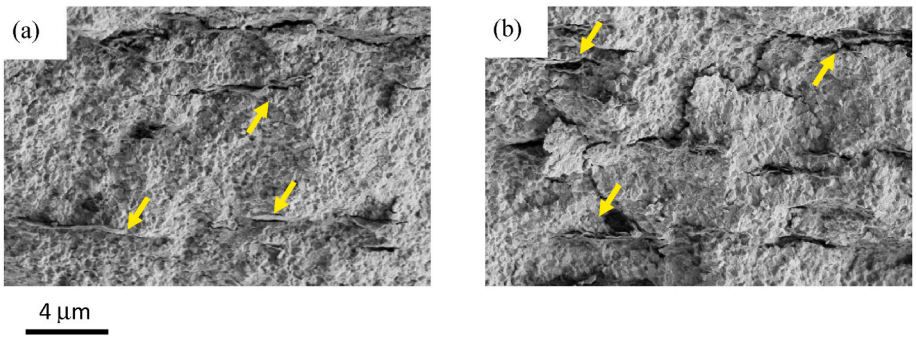

Fig. 3. SEM micrographs of the fracture surfaces of 2.5 vol% FLG-based nanocomposites prepared by (a) bath sonication and (b) wet milling.

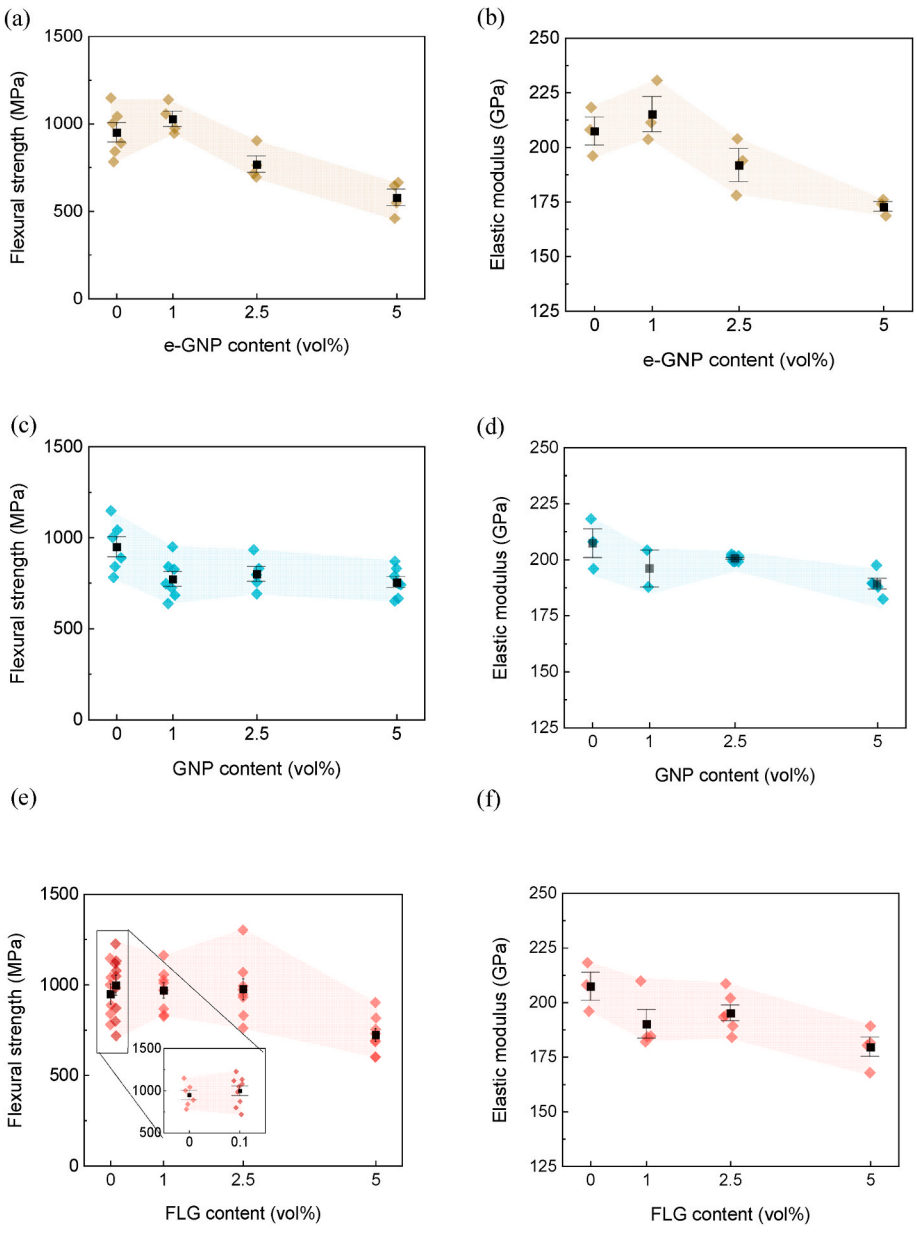

Fig. 4. Flexural strength and elastic modulus of (a, b) e-GNP, (c, d) GNP, and (e, f) FLG-based composites. The results for 1.0 and 5.0 vol% e-GNP have been previously published [37], but have been included for comparison.

dispersion of the FLG (Fig. 1d), which causes the presence of larger agglomerates [35]. An issue with respect to the fracture surfaces in *m*-FLG composites that supports this statement is that the microcavities opening along the interfaces between the nanostructures and the matrix during fracture, creating a microscopic gap between the FLGs and the ceramic grains, are more significant in FLG-filled composites when the nanostructures are dispersed by wet milling (Fig. 3). Additionally, the presence of overlapping FLGs leads to a lower reinforcement effectiveness of ceramic-matrix composites because the contact area at the interface of the nanofiller and the matrix diminishes as well as the friction forces [36]. These mechanisms will be deeply analysed in section 3.2.2.

3.2.2. *Influence of GBN aspect ratio and content*

To analyse how the aspect ratio and content of GBNs can affect the mechanical properties of the ceramic matrix composites, the flexural strength and elastic modulus of the FLG samples were compared to those of the e-GNP and GNP ones. These values are shown in Fig. 4. The properties of 3Y-TZP are included for comparison.

The results show that the flexural strength of the composites filled with e-GNPs (Fig. 4a and b) increases slightly to 1030 ± 100 MPa, compared to the ceramic matrix, when the filler content is 1 vol%, and reaches a maximum value of 1137 MPa (Table 1). However, above that percentage, it diminishes ~25 and ~43%, for e-GNP contents of 2.5 and 5.0 vol%, respectively. A similar tendency is obtained for the elastic modulus, where 1 vol% reinforced-composites are slightly stiffer than the 3Y-TZP ceramic, but higher contents cause a diminution of the stiffness. A similar behaviour has previously been observed in Al_2O_3-WC-TiC ceramic composites [35], where an improvement in flexural strength was observed with a maximum value at a GNP content of 0.5 vol% followed by an abrupt decrease for higher percentages. The detected diminution, in that case, was attributed to the presence of overlapping GNPs (sizes ranging from 0.5 up to 5 μm) and agglomerates, leading to the appearance of pores, degrading the mechanical performance of the material.

The existence of a critical nanofiller content has been found in not

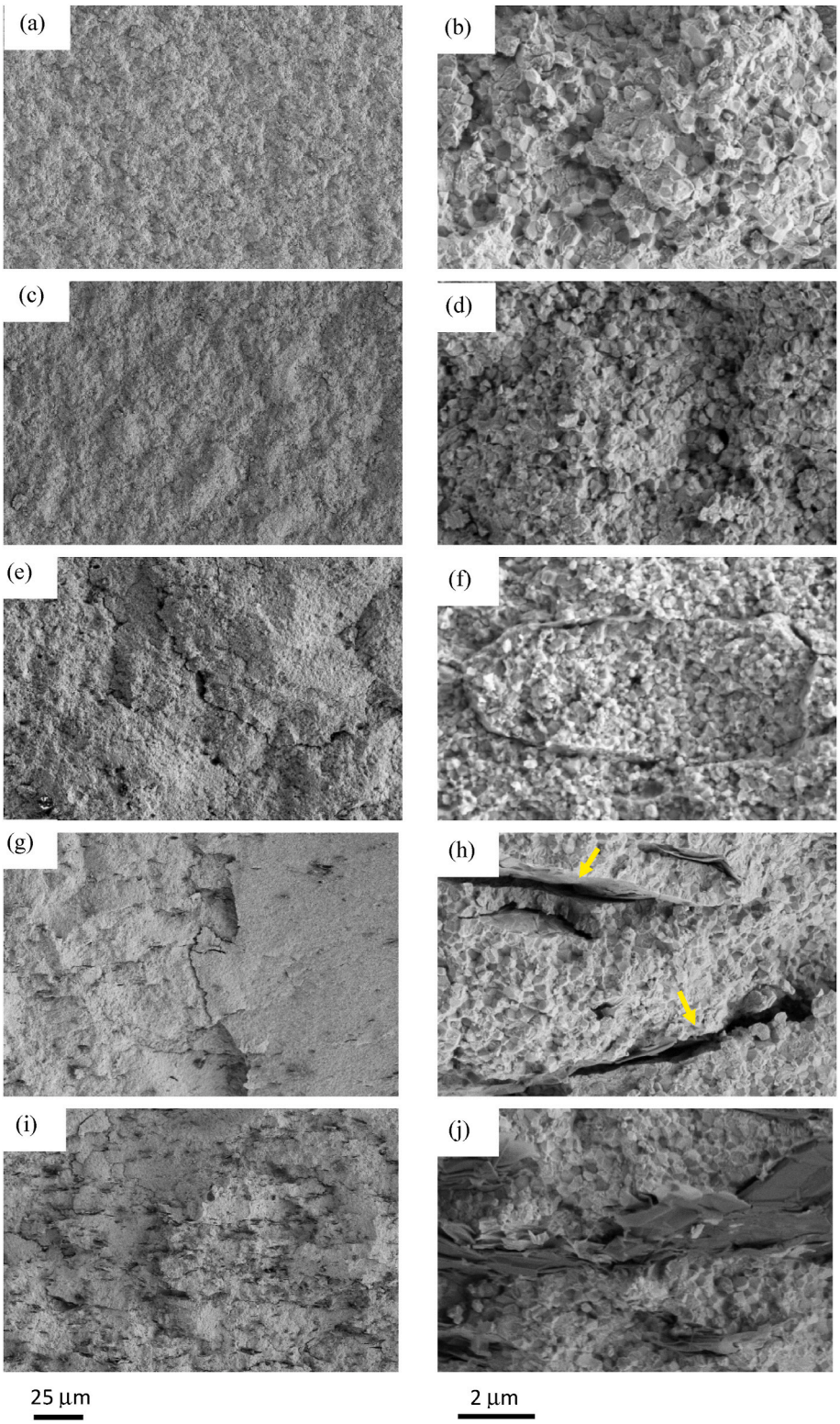

Fig. 5. SEM micrographs of the fracture surface of (a, b) 3Y-TZP and (c–j) GBN-based nanocomposites: (c–f) e-GNP with contents of (c, d) 1.0 vol% and (e, f) 5.0 vol %; and (g–j) GNP with contents of (g, h) 1.0 vol% and (i, j) 5.0 vol%.

only flexural strength, but also in toughness. Bobylev et al. [38] reported that the use of contents above 5 vol% induces clustering, which is the main reason for the observed decrease. Sun et al. [39] also agree with this idea, as they stated that higher contents than a critical threshold give rise to a low-quality degraded dispersion and an insufficient grain boundary surface to adequately host the GBNs.

Unlike the trend observed for e-GNPs, when using GNPs as filler (Fig. 4c and d), no enhancement in flexural strength was observed. However, an increase in the GNP content has no detrimental effect, keeping the flexural strength value mainly unchanged. This can be attributed to the combined higher lateral size and thickness of the GNPs, related to e-GNPs, as thicker GNPs are rigid and can favour the

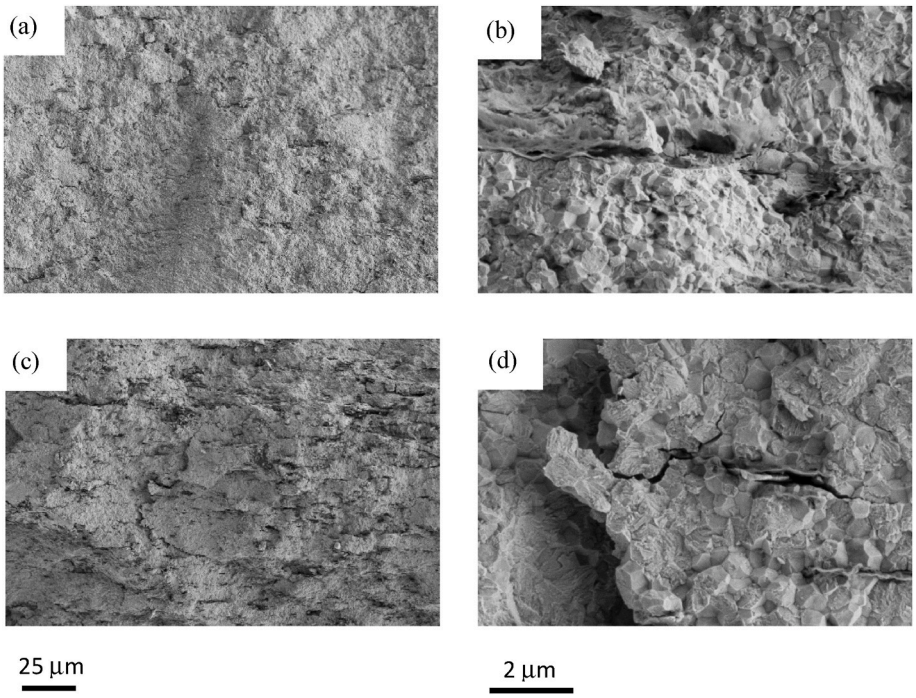

Fig. 6. Fracture surface of FLG-based nanocomposites: (a, b) 1.0 and (c, d) 5.0 vol%.

formation of microcavities along the GNP-ceramic matrix interfaces during fracture propagation, as mentioned above for FLG composites (Fig. 5h). The flattened surfaces observed in the matrix after pull-out of the GBN may also be indicative of the low interfacial strength. Obradović et al. [40] obtained a similar trend in composites with GNPs with sizes similar to those used in the present work. They observed smooth surfaces in areas previously covered by GNPs in fractography, which they attributed to the weak interface formed between the filler and the matrix, favoring crack propagation along it. Results published by Li et al. [41] also showed that, GNP/3Y-TZP composites experience toughening by adding GNP content up to 1.0 wt% (~2.6 vol%), while flexural strength progressively decreases from 1089 ± 10 MPa down to 975 ± 10 MPa up to fractions of 1.5 wt% (~3.9 vol%).

In the case of the FLG-based nanocomposites, the flexural strength (Fig. 4e and f) slightly increases up to an FLG content of 2.5 vol%, reaching a value of 980 ± 270 MPa, with a maximum of 1304 MPa. This enhancement (Weibull scale and shape parameter are available for additional information in Table 1) can be due to both the presence of wrinkled FLG and the lower thickness compared to GNP-based materials. The presence of wrinkles in graphene nanolayers has been reported to cause an increase of three times in the force needed for the pull-out, compared to flat graphene nanoplatelets [42]. Consequently, wrinkled laminar structures could contribute to hinder debonding at the interface [43], although the presence of wrinkles at triple grain junctions can lead to inefficient load transfer at the interfaces if they act as 2D pores in the composite [44].

Additionally, the improvement in flexural strength achieved by incorporating very low FLG contents was not as significant as some authors have reported [45]. The flexural strength obtained for composites filled with 0.1 vol% was 1000 ± 170 MPa, with a maximum value of 1132 MPa.

As in the case of e-GNPs, a critical content was observed in FLG-filled materials. This critical threshold has also been noticed by several authors who analysed the mechanical behaviour of similar systems. Li et al. [45] studied the response of GNP-reinforced 3Y-TZP ceramic. Although the contents were lower than those presented in this work, below 0.1 wt % (~0.3 vol%), they reported that the addition of GNPs increased both the stiffness and the flexural strength. However, the increase seemed only feasible up to a content of 0.03 wt% (~0.1 vol%), which is generally below the electrical percolation threshold of these systems [28,46]. Li et al. [47] also found a slight increase in flexural strength for low graphene-based nanostructure fractions, lower than 0.2 wt% (~0.5 vol%), in Al_2O_3–TiC matrix ceramic composites. In this case, the authors attributed the enhancement in the mechanical properties to the crack deflection, branching, bridging, and pull-out of the GBNs, as well as the refinement of the grain size.

To further analyse the mechanisms that take place, Figs. 5 and 6 show representative SEM micrographs of the fracture surfaces after the flexural tests of the 3Y-TZP ceramic, and the materials filled with 2.5 and 5.0 vol% GBNs. The fracture in 3Y-TZP occurs through both transgranular and intergranular propagation (Fig. 5a and b). These mechanisms can also be observed in GBN-based nanocomposites (Fig. 5c–j and 6).

The incorporation of e-GNP into the ceramic matrix causes a slight reduction in the grain size, as mentioned before, which is perceptible from the fracture surfaces and has been previously reported by the authors [37]. Due to the small lateral dimension of the nanoplatelets, the

Table 3
Roughness parameters of the fracture surfaces of GBN-based nanocomposites.

Composite	GBN content (vol%)	Mean roughness depth, R_z (µm)	Average roughness, R_a (µm)
3YTZP	–	0.60 ± 0.04	0.16 ± 0.01
FLG	0.1	–	–
	1	1.3 ± 0.4	0.37 ± 0.07
	2.5	1.33 ± 0.13	0.39 ± 0.01
	5	1.4 ± 0.4	0.41 ± 0.09
FLG-1300	2.5	–	–
m-FLG	2.5	–	–
m-FLG-100	2.5	–	–
e-GNP	1	0.47 ± 0.05	0.13 ± 0.02
	2.5	0.53 ± 0.05	0.14 ± 0.02
	5	0.94 ± 0.16	0.24 ± 0.04
GNP	1	1.15 ± 0.19	0.31 ± 0.08
	2.5	2.03 ± 0.5	0.46 ±0.07
	5	1.14 ± 0.14	0.31 ± 0.05

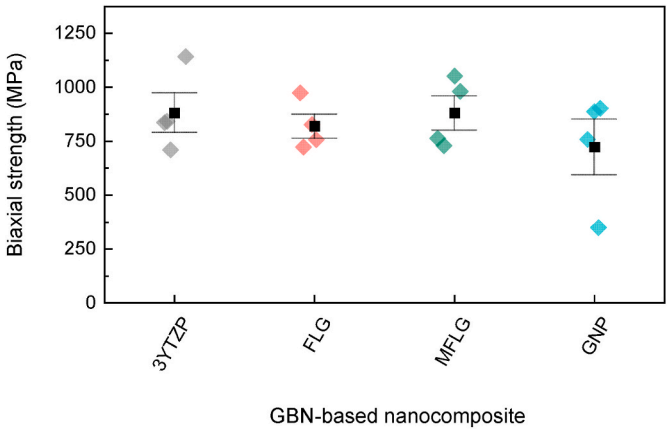

Fig. 7. Biaxial strength of GBN-based composites (2.5 vol%).

effective number of e-GNPs incorporated into the matrix is higher, compared with those of the other materials with the same GBN vol% analysed in this work, resulting in a more significant grain size refinement. In these composites, crack deflection and branching can be observed as dominant mechanisms to hinder crack propagation (Fig. 5c-f). Due to the high effective number of e-GNPs and their random orientation, tortuosity of the crack pathway is more accused than in the other cases, as the crack deviates when encountering an e-GNP, which contributes to the enhancement of the flexural strength. The deviation of the cracks occurs at a microscopic scale at short distances, resulting in relatively smooth fracture surfaces with R_a values of 0.12–0.24 μm and R_z below 1 μm.

In contrast, the fracture surface of GNP-based composites (Fig. 5g-i) shows significant GNP pull-out, which is the result of a weak bonding between the filler and the 3Y-TZP matrix [48] together with the flattened surface of adjacent ceramic grains already mentioned above. This is related to the combined high lateral size and thickness of the GNPs already mentioned above, which favours the formation of microcavities at the interfaces between the GNPs and the 3Y-TZP matrix during fracture and, consequently, the pull-out. The pores tend to appear at the vicinities and along the GBNs, which are placed in the grain boundaries, and act as the origin of the fracture [36]. This mechanism becomes more significant as the GNP content increases and seems to be the responsible for the flexural strength decrease previously stated, as cracks can easily propagate throughout the interfaces. Because of the pull-out and propagation of cracks throughout the interfaces of larger lateral size GNPs, related to e-GNPs, the roughness of the fracture surface (Table 3) increases up to ~0.31 and ~1.15 μm for R_a and R_z, respectively. Markandan et al. [18] also observed GNP pull-out as the dominant mechanism for crack deflection and toughening due to the formation of agglomerates for a GNP content greater than 2.0 wt% (~5.2 vol%).

For the FLG-filled composites, at low contents, the fracture surfaces are similar to those of the monolithic 3Y-TZP (Fig. 6a and b), where transgranular and intergranular crack propagation are the main mechanisms. Although some FLG pull-out can be seen, it seems that it has no detrimental effect on the flexural strength. The reason could reside in the FLGs with high $L_{GBN,}$ which locate covering groups of ceramic grains and present a wrinkled structure, promoting an anchoring effect. As a result of the wrinkled structure, the friction forces increase and so does the energy needed for crack propagation [49]. Although the FLG L_{GBN} and fracture surface roughness parameters are quite similar to the ones of GNPs, it is the lower thickness of the FLGs the key point in the flexural strength enhancement observed for contents below 2.5 vol%, since it allows the nanosheets surrounding the ceramic grains to be more flexible and adapt more closely to their shape, which seems to avoid the presence of microcavities at the interface between the FLGs and the ceramic matrix and makes difficult pull-out.

Due to the preferential orientation of the FLGs, crack deflection along the interfaces between the nanofiller and the 3Y-TZP occurs nearly perpendicular to the direction of the applied force. This is probably also contributing to the resultant strengthening described above. However, with higher FLG contents, pull-out becomes the dominant mechanism due to the reduction of the mean free path between the FLGs, which reduces the size of ceramic regions surrounded by FLG, and to the overlapping of the nanostructures (Fig. 6c and d). The lower distances between FLGs, the more connected network, and the presence of microcavities due to overlapping make crack propagation easier as it can move between the two phases along the weak interfaces creating three-dimensional paths [50].

It has been likewise found by Ahmad et al. [51] that the presence of folded graphene-based nanostructures and interconnected networks located at the grain boundaries favour crack propagation due to sliding in the basal plane. This grain boundary sliding has also been reported by Liu et al. [52] for rGO composites due to the weak bonding with the ceramic matrix, which promotes rGO behaviour as a lubricant network along the grain boundaries.

Similar results are obtained in the of biaxial strength, as observed in Fig. 7, where the results of the three composites with 2.5% composites are compared with 3YTZP. All samples presented values of biaxial strength in the 750–1000 MPa range, with a large scatter due to, probably, the inhomogeneities of the microstructure, as discussed before. Therefore, it can be concluded that the strength of the reinforced zirconia samples has values comparable to those of the unreinforced samples.

While the thicker fillers (GNPs) caused a decrease in the flexural strength for all the contents, the thinner ones (FLG) slightly strengthened for contents below 2.5 vol%. A similar effect than that of FLG was caused by the fragmentation of the GNP (e-GNP). Due to the lower thickness, they better accommodate along grain boundaries and enhance interfacial strength.

Although no significant enhancements in flexural and biaxial strength were found in the present study, the significance of the analysis reported in this work relies on the establishment of the maximum nanofiller contents as well as the best-fit geometries of GBNs to obtain multifunctional ceramic composite materials without a detrimental effect on the strength. It is well known that the addition of GBNs to ceramic matrices is interesting for applications where electrical and thermal conductivities are a priority [53,54], as already mentioned. Additionally, tribological properties are considerably improved due to the creation of a self-lubricating surface [55] when using relatively low filler contents.

4. Conclusions

An analysis of the flexural strength, biaxial strength, and fracture mechanisms of different GBN-based 3Y-TZP composites was carried out. Composites with FLG dispersed via bath sonication showed a slight increase in flexural strength and elastic modulus compared to the ceramic matrix up to a content of 2.5 vol%. However, the use of wet milling as the dispersion method led to a less dispersed filler (*m*-FLG), which resulted also in a lower interconnectivity between the FLGs and a significant opening of microcavities during fracture at the nanofiller-matrix interfaces. This induced a reduction in flexural strength. The different sintering heating rates used in this work did not show perceptible changes in mechanical properties. On the contrary, the increase in the sintering temperature of 100 °C, which made the composite with 2.5 vol % electrically conductive enabling multifunctionality, led to a slight decrease in flexural strength, which could be due to a slight increase in grain size and residual stresses.

The flexural strength and the elastic modulus of the composites filled with e-GNPs and FLGs was found to slightly increase up to filler contents of 1.0 and 2.5 vol%, respectively. This behaviour was attributed to the increase in the effective number of GBNs incorporated into the matrix,

the higher interfacial strength, and the higher tortuosity of the crack propagation paths due to deflection and branching. Above these filler contents, pores appear as a result of overlapping GBNs and agglomerates, promoting easier pull-out of the nanoplatelets, and thus leading to lower flexure strength values.

The incorporation of thicker GNPs with higher lateral size caused a decrease in both flexural strength and stiffness, probably due to the flat ceramic grain areas adjacent to the GNPs and low interfacial strength, which could also facilitate the GNP pull-out, and thus the crack propagation along them.

Declaration of competing interest

The authors declare that they have no known competing financial interests or personal relationships that could have appeared to influence the work reported in this paper.

Acknowledgements

This research was funded by MCIN/AEI/10.13039/501100011033 (Ministerio de Ciencia e Innovación, Spanish Government, Agencia Estatal de Investigación) [projects PGC2018-101377-B-100 and PID2022-140191NB-I0] and ERDF (European Regional Development Funding) "A way of making Europe", by the European Union and by [project P20_01024] (Junta de Andalucía/FEDER, UE 2014–2020). C. López-Pernía acknowledges the financial support of MINECO (Ministerio de Economía y Competitividad, Spanish Government) through a FPI contract [ref: BES-2016- 078711]. C. Muñoz-Ferreiro acknowledges the financial support of a VI PPIT-US (Plan Propio Universidad de Sevilla, Spain) fellowship [USE-18740-H].

During the preparation of this work the authors used *Writefull* in order to make English linguistic improvements. After using this tool/service, the author(s) reviewed and edited the content as needed and take full responsibility for the content of the publication.

References

[1] A. Datye, K.H. Wu, G. Gomes, V. Monroy, H.T. Lin, J. Vleugels, K. Vanmeensel, Synthesis, microstructure and mechanical properties of Yttria Stabilized Zirconia (3YTZP) - multi-Walled Nanotube (MWNTs) nanocomposite by direct in-situ growth of MWNTs on Zirconia particles, Compos. Sci. Technol. 70 (2010) 2086–2092, https://doi.org/10.1016/j.compscitech.2010.08.005.

[2] C. Baudín, J. Gurauskis, A.J. Sánchez-Herencia, V.M. Orera, Indentation damage and residual stress field in alumina-Y_2O_3-stabilized zirconia composites, J. Am. Ceram. Soc. 92 (2009) 152–160, https://doi.org/10.1111/j.1551-2916.2008.02813.x.

[3] M. Ji, J. Xu, L. Li, D. Yu, M. Chen, M. el Mansori, Nano-scale mechanical behaviors and material removal mechanisms of zirconia ceramics sintered at various temperatures, Ceram. Int. 47 (2021) 32588–32598, https://doi.org/10.1016/j.ceramint.2021.08.154.

[4] H. Porwal, S. Grasso, M.J. Reece, Review of graphene-ceramic matrix composites, Adv. Appl. Ceram. 112 (2013) 443–454, https://doi.org/10.1179/174367613X13764308970581.

[5] E. Hosseini, M. Zakertabrizi, A. Habibnejad Korayem, R. Shahsavari, Tunable, multifunctional ceramic composites via intercalation of fused graphene boron nitride nanosheets, ACS Appl. Mater. Interfaces 11 (2019) 8635–8644, https://doi.org/10.1021/acsami.8b19409.

[6] Y. Huang, C. Wan, Controllable fabrication and multifunctional applications of graphene/ceramic composites, Journal of Advanced Ceramics 9 (2020) 271–291, https://doi.org/10.1007/s40145-020-0376-7.

[7] J. Tao, J. Wang, Q. Zeng, A comparative study on the influences of CNT and GNP on the piezoresistivity of cement composites, Mater. Lett. 259 (2020) 126858, https://doi.org/10.1016/j.matlet.2019.126858.

[8] M. Drozdova, I. Hussainova, D. Pérez-Coll, M. Aghayan, R. Ivanov, M.A. Rodríguez, A novel approach to electroconductive ceramics filled by graphene covered nanofibers, Mater. Des. 90 (2016) 291–298, https://doi.org/10.1016/j.matdes.2015.10.148.

[9] A. Rincón, R. Moreno, A.S.A. Chinelatto, C.F. Gutierrez, E. Rayón, M.D. Salvador, A. Borrell, Al_2O_3-3YTZP-Graphene multilayers produced by tape casting and spark plasma sintering, J. Eur. Ceram. Soc. 34 (2014) 2427–2434, https://doi.org/10.1016/j.jeurceramsoc.2014.02.011.

[10] J. Gao, Q. Ding, P. Yan, Y. Liu, J. Huang, T. Mustafa, R. Guo, X. Lu, K. Wang, S. Sun, X. Feng, W. Luo, Y. Fan, W. Jiang, Highly improved microwave absorbing and mechanical properties in cold sintered ZnO by incorporating graphene oxide, J. Eur. Ceram. Soc. 42 (2022) 993–1000, https://doi.org/10.1016/j.jeurceramsoc.2021.10.053.

[11] A. Kishimoto, Y. Takagawa, T. Teranishi, H. Hayashi, Effect of varying the ratio of matrix/dispersoid particle size on the piezoresistivity of alumina/carbon-black composite ceramics, Mater. Lett. 65 (2011) 2197–2200, https://doi.org/10.1016/j.matlet.2011.04.042.

[12] K. Waku, H. Hayashi, A. Kishimoto, Resistivity of alumina-graphite composite ceramics, J. Am. Ceram. Soc. 91 (2008) 4168–4170, https://doi.org/10.1111/j.1551-2916.2008.02820.x.

[13] F. Chen, K. Yan, J. Sun, J. Hong, Y. Zhu, Z. Huang, From the research state of the thermal properties of graphene reinforced ceramics to the future of computer simulation, Ceram. Int. 46 (2020) 18428–18445, https://doi.org/10.1016/j.ceramint.2020.04.265.

[14] M. Zhou, T. Lin, F. Huang, Y. Zhong, Z. Wang, Y. Tang, H. Bi, D. Wan, J. Lin, Highly conductive porous graphene/ceramic composites for heat transfer and thermal energy storage, Adv. Funct. Mater. 23 (2013) 2263–2269, https://doi.org/10.1002/adfm.201202638.

[15] M. Zhou, H. Bi, T. Lin, X. Lü, F. Huang, J. Lin, Directional architecture of graphene/ceramic composites with improved thermal conduction for thermal applications, J Mater Chem A Mater 2 (2014) 2187–2193, https://doi.org/10.1039/c3ta14325b.

[16] C. Muñoz-Ferreiro, C. López-Pernía, R. Moriche, A. Gommeringer, F. Kern, R. Poyato, Gallardo-López, Highly efficient electrical discharge machining of yttria-stabilized zirconia ceramics with graphene nanostructures as fillers, J. Eur. Ceram. Soc. 42 (2022) 5943–5952, https://doi.org/10.1016/j.jeurceramsoc.2022.06.037.

[17] B.K. Jang, J.H. Lee, C.A.J. Fisher, Mechanical properties and phase-transformation behavior of carbon nanotube-reinforced yttria-stabilized zirconia composites, Ceram. Int. 47 (2021) 35287–35293, https://doi.org/10.1016/j.ceramint.2021.09.071.

[18] K. Markandan, M.T.T. Tan, J. Chin, S.S. Lim, A novel synthesis route and mechanical properties of Si-O-C cured Yytria stabilised zirconia (YSZ)-graphene composite, Ceram. Int. 41 (2015) 3518–3525, https://doi.org/10.1016/j.ceramint.2014.11.008.

[19] F. Chen, D. Jin, K. Tyeb, B. Wang, Y.-H. Han, S. Kim, J.M. Schoenung, Q. Shen, L. Zhang, Field assisted sintering of graphene reinforced zirconia ceramics, Ceram. Int. 41 (2015) 6113–6116, https://doi.org/10.1016/j.ceramint.2014.12.147.

[20] J. Liu, H. Guo, Y. Su, L. Wang, L. Wei, G. Yang, Y. Yang, K. Jiang, Spark plasma sintering of graphene platelet reinforced zirconia composites with improved mechanical performance, Mater. Sci. Eng. 688 (2017) 70–75, https://doi.org/10.1016/j.msea.2017.01.107.

[21] Y. Cui, B. Chen, G. Xiao, M. Yi, J. Zhang, H. Chen, T. Zhou, Z. Chen, J. Wu, C. Xu, Mechanical properties and cutting performance of laminated graphene composite ceramic tools, J. Manuf. Process. 81 (2022) 717–726, https://doi.org/10.1016/j.jmapro.2022.06.076.

[22] Q. Lin, H. Chen, G. Xiao, M. Yi, Z. Chen, J. Zhang, C. Xu, J. Wu, Effect of graphene nanoplatelets on the mechanical properties and cutting performance of alumina nanocomposite ceramic tools prepared using the SPS-HF dual sintering method, Ceram. Int. 48 (2022) 19240–19249, https://doi.org/10.1016/j.ceramint.2022.03.216.

[23] X. Sun, W. Wang, G. Sun, J. Chen, L. Wang, J. Bi, Enhancement of the mechanical properties of nacre-like alumina ceramic by the synergism of graphene oxide and Si_3N_4 whisker, Ceram. Int. 48 (2022) 941–946, https://doi.org/10.1016/j.ceramint.2021.09.178.

[24] C.G. Barbosa Pereira, F.D. Faglioni, V.G. Neto, C.A. Fortulan, R.V. Gelamo, C. R. Foschini, Reducing atmosphere to manufacture graphene alumina composite, Ceram. Int. 48 (2022) 17143–17148, https://doi.org/10.1016/j.ceramint.2022.02.270.

[25] J. Wu, W. Xu, T. Dong, M. Jin, Y. Zhou, Self-assembly of graphene reinforced ZrO_2 composites with deformation-sensing performance, Ceram. Int. 48 (2022) 32131–32142, https://doi.org/10.1016/j.ceramint.2022.07.153.

[26] C. Zhang, Z. Jiang, L. Zhao, W. Liu, P. Si, J. Lan, Synthesis and characterization of multilayer graphene oxide on yttria-zirconia ceramics for dental implant, J. Mater. Res. 35 (2020) 2466–2477, https://doi.org/10.1557/jmr.2020.199.

[27] S. Ramesh, M.M. Khan, H.C. Alexander Chee, Y.H. Wong, P. Ganesan, M.G. Kutty, U. Sutharsini, W.J.K. Chew, A. Niakan, Sintering behaviour and properties of graphene oxide-doped Y-TZP ceramics, Ceram. Int. 42 (2016) 17620–17625, https://doi.org/10.1016/j.ceramint.2016.08.077.

[28] A. Gallardo-López, I. Márquez-Abril, A. Morales-Rodríguez, A. Muñoz, R. Poyato, Dense graphene nanoplatelet/yttria tetragonal zirconia composites: processing, hardness and electrical conductivity, Ceram. Int. 43 (2017) 11743–11752, https://doi.org/10.1016/j.ceramint.2017.06.007.

[29] C. López-Pernía, C. Muñoz-Ferreiro, C. González-Orellana, A. Morales-Rodríguez, Gallardo-López, R. Poyato, Optimizing the homogenization technique for graphene nanoplatelet/yttria tetragonal zirconia composites: influence on the microstructure and the electrical conductivity, J. Alloys Compd. 767 (2018) 994–1002, https://doi.org/10.1016/j.jallcom.2018.07.199.

[30] M. Zhao, D.B. Xiong, Z. Tan, G. Fan, Q. Guo, C. Guo, Z. Li, D. Zhang, Lateral size effect of graphene on mechanical properties of aluminum matrix nanolaminated composites, Scripta Mater. 139 (2017) 44–48, https://doi.org/10.1016/j.scriptamat.2017.06.018.

[31] A.G. Sheinerman, Modeling of structure and interface controlled strength of laminated metal/graphene composites, Mech. Mater. 158 (2021), https://doi.org/10.1016/j.mechmat.2021.103888.

[32] C. Muñoz-Ferreiro, C. López-Pernía, Á. Gallardo-López, R. Poyato, Unravelling the optimization of few-layer graphene crystallinity and electrical conductivity in ceramic composites by Raman spectroscopy, J. Eur. Ceram. Soc. (2021), https://doi.org/10.1016/j.jeurceramsoc.2021.09.025.

[33] A.G. Sheinerman, Modeling of fracture toughness enhancement and reduction in fully dense ceramic/graphene composites, Eur. J. Mech. Solid. 98 (2023), https://doi.org/10.1016/j.euromechsol.2022.104891.
[34] C. López-Pernía, C. Muñoz-Ferreiro, R. Moriche, A. Morales-Rodríguez, Gallardo-López, R. Poyato, Electrical performance of orthotropic and isotropic 3YTZP composites with graphene fillers, J. Eur. Ceram. Soc. 43 (2023) 1605–1612, https://doi.org/10.1016/j.jeurceramsoc.2022.11.068.
[35] X. Wang, J. Zhao, E. Cui, S. Song, H. Liu, W. Song, Microstructure, mechanical properties and toughening mechanisms of graphene reinforced Al_2O_3 -WC-TiC composite ceramic tool material, Ceram. Int. 45 (2019) 10321–10329, https://doi.org/10.1016/j.ceramint.2019.02.087.
[36] J. Liu, H. Yan, K. Jiang, Mechanical properties of graphene platelet-reinforced alumina ceramic composites, Ceram. Int. 39 (2013) 6215–6221, https://doi.org/10.1016/j.ceramint.2013.01.041.
[37] Á. Gallardo-López, J. Castillo-Seoane, C. Muñoz-Ferreiro, C. López-Pernía, A. Morales-Rodríguez, R. Poyato, Flexure strength and fracture propagation in zirconia ceramic composites with exfoliated graphene nanoplatelets, Ceramics 3 (2020) 78–91, https://doi.org/10.3390/ceramics3010009.
[38] S.V. Bobylev, A.G. Sheinerman, Effect of crack bridging on the toughening of ceramic/graphene composites, Rev. Adv. Mater. Sci. 57 (2018) 54–62, https://doi.org/10.1515/rams-2018-0047.
[39] J. Sun, J. Zhao, Y. Chen, L. Wang, X. Yun, Z. Huang, Macro-micro-nano multistage toughening in nano-laminated graphene ceramic composites, Materials Today Physics 22 (2022), https://doi.org/10.1016/j.mtphys.2021.100595.
[40] N. Obradović, F. Kern, Properties of 3Y-TZP zirconia ceramics with graphene addition obtained by spark plasma sintering, Ceram. Int. 44 (2018) 16931–16936, https://doi.org/10.1016/j.ceramint.2018.06.133.
[41] S. Li, Z. Xie, Y. Zhang, Y. Zhou, Enhanced toughness of zirconia ceramics with graphene platelets consolidated by spark plasma sintering, Int. J. Appl. Ceram. Technol. 14 (2017) 1062–1068, https://doi.org/10.1111/ijac.12742.
[42] S. Zhao, Y. Zhang, J. Yang, S. Kitipornchai, Significantly improved interfacial shear strength in graphene/copper nanocomposite via wrinkles and functionalization: a molecular dynamics study, Carbon N Y 174 (2021) 335–344, https://doi.org/10.1016/j.carbon.2020.12.026.
[43] X. Wang, J. Zhao, E. Cui, X. Tian, Z. Sun, Effect of interfacial structure on mechanical properties of graphene reinforced Al_2O_3–WC matrix ceramic composite, Nanomaterials 11 (2021), https://doi.org/10.3390/nano11061374.
[44] Y. Fan, G. Igarashi, W. Jiang, L. Wang, A. Kawasaki, Highly strain tolerant and tough ceramic composite by incorporation of graphene, Carbon N Y 90 (2015) 274–283, https://doi.org/10.1016/j.carbon.2015.04.029.
[45] Y. Li, F. Chen, Q. Shen, L. Zhang, Microstructure and mechanical behavior of zirconia ceramics by graphene nano-platelets incorporation, Mater. Res. Express 6 (2019), https://doi.org/10.1088/2053-1591/ab3181.
[46] O.Y. Kurapova, A.G. Glukharev, O.V. Glumov, M.Y. Kurapov, E.V. Boltynjuk, V. G. Konakov, Structure and electrical properties of YSZ-rGO composites and YSZ ceramics, obtained from composite powder, Electrochim. Acta 320 (2019), https://doi.org/10.1016/j.electacta.2019.134573.
[47] Z. li Li, J. Zhao, J. lin Sun, F. Gong, X. ying Ni, Reinforcing effect of graphene on the mechanical properties of Al_2O_3/TiC ceramics, Int. J. Miner. Metall. Mater. 24 (2017) 1403–1411, https://doi.org/10.1007/s12613-017-1533-z.
[48] X. Wang, J. Zhao, E. Cui, H. Liu, Y. Dong, Z. Sun, Effects of sintering parameters on microstructure, graphene structure stability and mechanical properties of graphene reinforced Al_2O_3-based composite ceramic tool material, Ceram. Int. 45 (2019) 23384–23392, https://doi.org/10.1016/j.ceramint.2019.08.040.
[49] B. Yazdani, Y. Xia, I. Ahmad, Y. Zhu, Graphene and carbon nanotube (GNT)-reinforced alumina nanocomposites, J. Eur. Ceram. Soc. 35 (2015) 179–186, https://doi.org/10.1016/j.jeurceramsoc.2014.08.043.
[50] Z. Zeng, Y. Liu, W. Chen, X. Li, Q. Zheng, K. Li, R. Guo, Fabrication and properties of in situ reduced graphene oxide-toughened zirconia composite ceramics, J. Am. Ceram. Soc. 101 (2018) 3498–3507, https://doi.org/10.1111/jace.15483.
[51] I. Ahmad, M. Islam, H.S. Abdo, T. Subhani, K.A. Khalil, A.A. Almajid, B. Yazdani, Y. Zhu, Toughening mechanisms and mechanical properties of graphene nanosheet-reinforced alumina, Mater. Des. 88 (2015) 1234–1243, https://doi.org/10.1016/j.matdes.2015.09.125.
[52] L. Liu, Y. Wang, X. Li, L. Xu, X. Cao, Y. Wang, Z. Wang, C. Meng, W. Zhu, X. Ouyang, Enhancing toughness in boron carbide with reduced graphene oxide, J. Am. Ceram. Soc. 99 (2016) 257–264, https://doi.org/10.1111/jace.13943.
[53] J. Ru, Y. Fan, W. Zhou, Z. Zhou, T. Wang, R. Liu, J. Yang, X. Lu, J. Wang, C. Ji, L. Wang, W. Jiang, Electrically conductive and mechanically strong graphene/mullite ceramic composites for high-performance electromagnetic interference shielding, ACS Appl. Mater. Interfaces 10 (2018) 39245–39256, https://doi.org/10.1021/acsami.8b12933.
[54] T. Mustafa, Y. Liu, J. Gao, P. Yan, Q. Ding, Y. Fan, W. Jiang, Highly aligned reduced graphene oxide in alumina composites for strengthening, toughening, and electromagnetic interference shielding, Journal of Materiomics 9 (2023) 993–1003, https://doi.org/10.1016/j.jmat.2023.03.005.
[55] A.R. Marlinda, G.S.H. Thien, M. Shahid, T.Y. Ling, A. Hashem, K.Y. Chan, M. R. Johan, Graphene as a lubricant additive for reducing friction and wear in its liquid-based form, Lubricants 11 (2023), https://doi.org/10.3390/lubricants11010029.